to have been observed.) It is hard to know how reliable the quantitative aspects of our model for the torsional motion in N_2O_5 are because the consequences of the high correlations which were found to exist between some parameters of the potential were not explored. (The pairs U_0, n and U_0, V_0 have correlation coefficients greater than 0.6.) We do feel that the model correctly describes the torsional behavior of N_2O_5 molecules in a semiquantitative sense, but detailed conclusions based on our values for the parameters of eq 1 must be drawn with caution.

Finally, it is worth noting that the gas-phase structure of N_2O_5 is altogether different from its structure in the crystal[24] where linear nitronium and planar nitrate ions are arranged in layers with the axes of the former perpendicular to the planes of the latter. In view of the ionic structure of the crystal and the covalent structure of the gas molecule, the high volatility of the solid is indeed remarkable.

Acknowledgment. We are indebted to the National Science Foundation which supported this work under grants CHE78-04258 and CHE81-10541. B.W.M. is grateful to Central Oregon Community College for a summer stipend.

Registry No. N_2O_5, 10102-03-1.

Supplementary Material Available: Tables of symmetry coordinates and force constants for N_2O_5, total scattered intensities and calculated backgrounds for each plate, and averaged molecular intensities (14 pages). Ordering information is given on any current masthead page.

(24) Grison, E.; Eriks, K., de Vries, J. L. *Acta Crystallogr.* **1950**, *3*, 290.

High-Pressure Collisional Activation Mass Spectrometry

Karl Blom and Burnaby Munson*

Contribution from the Department of Chemistry, University of Delaware, Newark, Delaware 19711. *Received December 10, 1982*

Abstract: Ions produced under chemical ionization (CI) conditions can be collisionally activated and dissociated within the high-pressure ion source by the application of relatively large electric fields within the source. A new multiregion ion source that separates regions of CI reaction and high-pressure collisional activation (HPCA) is employed to study these processes. These HPCA spectra may differ significantly from single-collision CID spectra of protonated species. Reactions between fragment ions and the reagent/collision gas are observed that can be used to differentiate the structures of fragment ions. Both parent and fragment ions can be analyzed by high-resolution mass spectrometry under HPCA conditions. Dissociation mechanisms are investigated and analytical applications discussed.

Introduction

Chemical ionization (CI) mass spectra frequently contain ions characteristic of the molecular weights of the samples and fragment ions that provide some structural information. The extent of fragmentation in CI mass spectra is generally less than the extent of fragmentation in electron ionization (EI) mass spectra. Class-characteristic ions of the same mass (31 for alcohols, 127 for iodides, 77 for alkylbenzenes, etc.) are generally absent in CI mass spectra. The extent of fragmentation can be readily changed by using different reactant ions. The weaker the reactant ion is as a Brønsted or Lewis acid, the smaller the extent of decomposition of the $(M + H)^+$ or $(M - H)^+$ ions from the sample.[1,2] The smaller the recombination energy of the charge-exchange reactant ion, the smaller the extent of fragmentation of the $M^{+\cdot}$ ions from the samples.[3]

Much research in CI mass spectrometry during the past several years has been directed toward the development of low-energy reactant ions that give only one ionic species per compound. The NH_3 and i-C_4H_{10} spectra of many compounds, for example, are essentially one species spectra, $(M + NH_4)^+$ or $(M + H)^+$. No structural information is provided by these spectra. Individual components have been identified in complex mixtures without prior separation by the use of CIMS to produce $(M + H)^+$ ions for each component. These $(M + H)^+$ ions can be separated and collisionally dissociated to give characteristic fragmentation patterns by MS/MS. This combination has proved very useful for the identification of structures of molecules.[4,5]

In addition to these low-pressure collisional activation or collisionally induced decompositions, similar decompositions have also been reported at high pressures within the source of a mass spectrometer. Very marked increases in fragmentation with increasing repeller voltages were reported several years ago for i-C_4H_{10} spectra of a few compounds.[6] Recently, collisionally activated decompositions within a drift tube source of a mass spectrometer were reported.[7] By changing the field strength within the source, the extent of fragmentation could be varied over a wide range; from virtually no fragmentation to virtually complete fragmentation.

In the earlier work, sample ion production and collisional activation occurred within the same space. Although it was clear that the increased fragmentation resulted primarily from collisional activation of the $(M + H)^+$ ions from the samples, there were possible major effects from the changes in the reactant ion distribution as the field strength in the source was changed. Because the dissociation reactions occur at high pressures, reactions of sample fragment ions with the reagent gas are also possible. We report here a flexible multiregion ion source that effectively separates the region of sample ion production from the region of high-pressure collisional activation (HPCA). Principles and some applications of high-pressure collisional activation will be discussed.

(1) Leung, H. W.; Harrison, A. G. *Can. J. Chem.* **1976**, *54*, 3439–3452.
(2) Herman, J. A.; Harrison, A. G. *Org. Mass Spectrom.* **1981**, *16*, 423–427.
(3) Sunner, J.; Szabo, I. *Int. J. Mass Spectrom., Ion Phys.* **1977**, *25*, 241–261.
(4) Hass, J. R.; Harvan, D. J.; Bursey, M. M. *Anal. Chim. Acta* **1979**, *105*, 129–137.
(5) (a) Hunt, D. F.; Shabanowitz, J.; Giordani, A. B. *Anal. Chem.* **1980**, *52*, 386–390. (b) Kondrat, R. W.; Cooks, R. G. *Ibid.* **1978**, *50*, 81A–92A. (c) Illies, A. J.; Llu, S.; Bowers, M. T. *J. Am. Chem. Soc.* **1981**, *103*, 5674–5676. (d) Yost, R. A.; Enke, C. G.; McGilvery, D. C.; Smith, D.; Morrison, J. D. *Int. J. Mass Spectrom., Ion Phys.* **1979**, *30*, 127–136. (e) Cody, R. B.; Burnier, R. C.; Freiser, B. S. *Anal. Chem.* **1982**, *54*, 96–101.
(6) Michnowicz, J.; Munson, B. *Org. Mass Spectrom.* **1970**, *4*, 481.
(7) Price, P. C.; Swofford, H. S.; Buttrill, S. E. *Anal. Chem.* **1977**, *49*, 1497–1500.

0002-7863/83/1505-3793$01.50/0

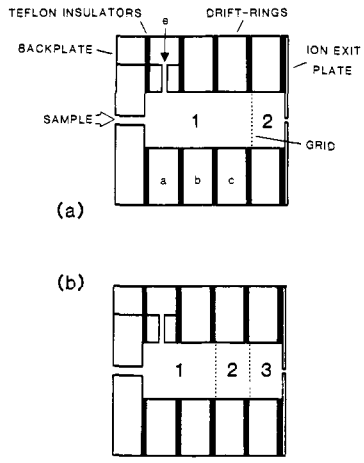

Figure 1. Multiregion ion source: (a) two-region configuration; (b) three-region configuration.

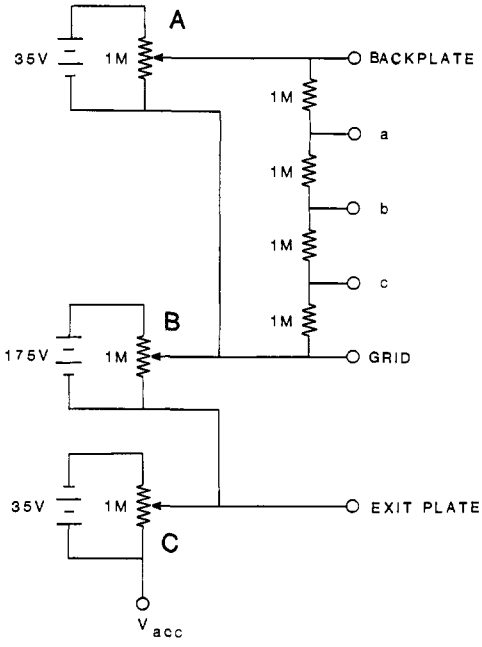

Figure 2. Circuitry for controlling potentials within the two-region ion source.

Experimental Section

All experiments were done by using a DuPont CEC 21-110B double-focusing mass spectrometer that has been modified for high-pressure operation.[8] A two-region configuration of the multiregion ion source is shown in Figure 1a. A partial description of this source has been given previously.[9] The source is made from Al drift rings separated by Teflon spacers. The interior surfaces of the Al source parts are gold-plated to reduce surface reactivity and provide a highly conductive surface. The stack is held tightly together with four 6–40 threaded rods. The Teflon spacers make seals sufficiently tight to achieve CI pressures of approximately 1 torr. The source chamber, in this mode of operation, is divided into two regions by a fine mesh (100–200 lines/in.) high-transparency (≥78%) wire grid. The grid covers the entire lateral cross section of the source chamber and is in electrical contact with the adjacent drift ring.

The potentials within the two-region source are supplied and controlled by the circuit shown in Figure 2. The potential differences between the backplate and grid (region 1) and the grid and ion exit plate (region 2) are controlled independently with potentiometers A and B, respectively. A voltage divider consisting of four 1-MΩ resistors mounted directly on the source controls the relative potentials of drift rings a–c (Figure 1a) producing a more uniform potential gradient within region 1. The ion exit plate can be biased relative to the accelerating voltage with potentiometer C. Small biasing voltages can increase the current of the ion beam, presumably by offsetting excess kinetic energy that the ions have acquired from the fields within the source.

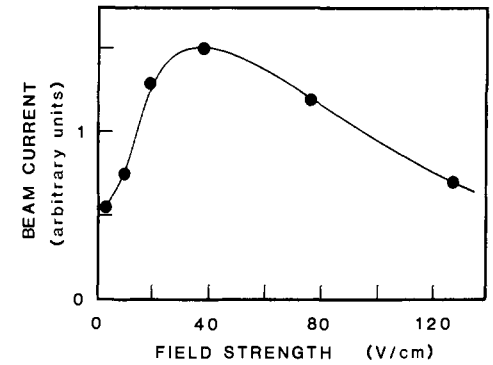

Figure 3. Total collectible ion current as a function of field strength in region 2 of the two-region source.

Electron energies of 400–500 V are generally used. Sensitivity is sufficient under these conditions for operation with a conventional Galileo Channeltron electron multiplier and our GC/MS data system.[10]

The dimensions of the ion source can be changed by the addition or removal of drift rings. The source can easily be altered to operate in other useful configurations. Removal of the grid gives a drift-tube ion source similar to the one described earlier by Buttrill.[7] Addition of a second grid gives a three region ion source, Figure 1b, which is useful in studying subsequent reactions of dissociation products with the reagent/collision gas.

At present the source is not heated and operates at 55–60 °C.

A low-field strength (5–10 V/cm) is maintained in region 1. Sample ions are produced in this region by CI reactions. These parent ions enter region 2, where they are accelerated in the applied field (10–200 V/cm) and undergo multiple collisions with reagent/collision gas molecules. In a collision, part of the kinetic energy of the ions is transfered into internal modes. Under high-pressure conditions only a small amount of kinetic energy is acquired from the field between collisions.[11] In general, a single activating collision will not convert sufficient kinetic energy into vibrational energy to dissociate the ions. The ions continue to increase their internal energy through subsequent accelerations and collisions until sufficient energy has accumulated and dissociation occurs. After dissociation the daughter ions are accelerated by the electric field and collisionally activated. Under sufficiently energetic conditions, daughter ions may then dissociate, giving rise to granddaughter ions. This sequence continues until the ions are finally extracted from region 2. In the two-region configuration of the source, Figure 1a, these ions leave the source and are mass analyzed to give the HPCA mass spectrum. In the three region configuration, Figure 1b, the ions leaving region 2 enter a third region in which they can react further with the reagent/collision gas. A low-field strength is maintained in region 3 so that the ions have a relatively large reaction time and no further activation occurs.

The long ionic path length of region 1 (d = 2.1 cm) results in a very large extent of reaction of the CI reactant ions with the sample. Sample concentrations are chosen such that essentially all of the reactant ions are converted to sample ions. Thus, sample ion production is effectively limited to region 1 and physically separated from the collisionally activated processes in region 2. The length of region 1 is limited in our system by the collectible beam current, which decreases approximately as the square of source length. The length of regions 2 and 3 were 0.8 cm for all the work reported here.

The collectible ion current depends on the field strength in region 2 as illustrated in Figure 3. The decrease in beam current at very high field strengths dictates the maximum usable field strength in region 2, about 200 V/cm for our system.

Results and Discussion

Figure 4 shows the effects of varying the field strength in region 2 of the two-region source on the distribution of ions from a mixture of 5% C_2H_6 in CH_4 at a total pressure of 0.42 torr. The field strength in region 1 was held constant at 10 V/cm throughout the experiment. At low-field strengths in region 2, below about 15 V/cm, the distribution of ionic abundances is essentially independent of the applied field. The observed ions are the same

(8) Hatch, F.; Munson, B. *J. Phys. Chem.* **1978**, *82*, 2362–2369.
(9) Blom, K.; Hilliard, L. J.; Gold, H. S.; Munson, B. *Anal. Chem.* **1982**, *54*, 1898–1899.
(10) Polley, C. W., Jr. Ph.D. Dissertation, University of Delaware, 1980.
(11) Kambara, H.; Kanomata, I. *Int. J. Mass Spectrom., Ion Phys.* **1977**, *25*, 129–136.

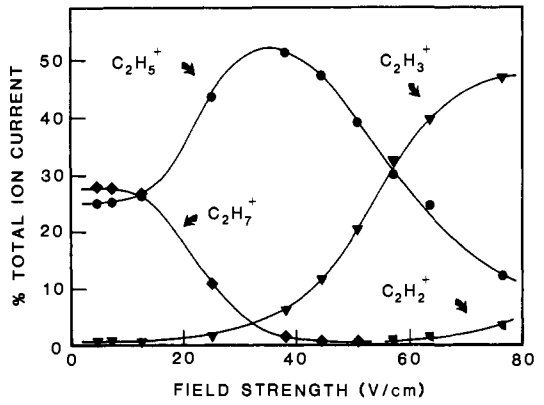

Figure 4. Relative abundances of the major ions from a 5% C_2H_6 in CH_4 mixture at a total pressure of 0.42 torr as a function of field strength in region 2 of the two-region source.

as those reported previously for C_2H_6/CH_4 mixtures: predominantly $C_2H_5^+$ from the reaction of CH_3^+ with CH_4 and from dissociative proton transfer from CH_5^+ to C_2H_6 and $C_2H_7^+$ from proton transfer from CH_5^+ to C_2H_6.[12] No collisionally activated dissociations are occurring at these field strengths.

At a critical field strength, E_c, of about 15 V/cm, there is a decrease in the relative abundance of $C_2H_7^+$ and an equal increase in the relative abundance of $C_2H_5^+$ that mark the onset of the collisionally activated dissociation shown in eq 1. The dissociation

$$C_2H_7^+ \xrightarrow[*]{CH_4} C_2H_5^+ + H_2 \quad D = 0.3 \text{ eV} \qquad (1)$$

energy, D, has been calculated from the ground-state heats of formation of the ions and represents the lower limit for the energy $C_2H_7^+$ must accumulate to decompose by reaction 1. Reaction 1 may be considered as a two-step process involving collisional activation followed by unimolecular dissociation:

$$C_2H_7^+ \xrightarrow{CH_4} C_2H_7^{+*} \qquad (1a)$$

$$C_2H_7^{+*} \rightarrow C_2H_5^+ + H_2 \qquad (1b)$$

The extent of dissociation depends on the rate of reaction 1b and the residence time of the excited ion, $C_2H_7^{+*}$, within region 2. At the critical field strength $C_2H_7^+$ acquires the minimum energy needed to dissociate just before it leaves region 2. The excited ion has a very short time to dissociate, and hence the extent of dissociation is small. As the field strength is increased, $C_2H_7^+$ accumulates the minimum energy needed to dissociate in fewer collisions and has a longer time within region 2 to dissociate; therefore, the extent of dissociation is larger. Metastable spectra of these ions have not been studied under these conditions.

Additional ions of lower mass and higher energy are produced as the field strength in region 2 is increased further. The critical field strength for the formation of $C_2H_3^+$ is about 35 V/cm and for $C_2H_2^+$ is about 90 V/cm. In studies under comparable conditions, but to much higher field strengths, the ion C_2H^+ is observed at a critical field strength of approximately 160 V/cm. We postulate that these ions are produced in a step-wise dissociation sequence (eq 2–4). Consecutive dissociation processes have been

$$C_2H_5^+ \xrightarrow[*]{CH_4} C_2H_3^+ + H_2 \quad D = 2.1 \text{ eV} \qquad (2)$$

$$C_2H_3^+ \xrightarrow[*]{CH_4} C_2H_2^+ + H \quad D = 4.4 \text{ eV} \qquad (3)$$

$$C_2H_2^+ \xrightarrow[*]{CH_4} C_2H^+ + H \quad D = 5.8 \text{ eV} \qquad (4)$$

observed in MS/MS/MS instruments[13] and in MS/MS instruments at higher gas pressures. The proposed sequence, eq 2–4, is supported by the failure to observe the competing higher energy dissociation of $C_2H_5^+$ (eq 5) under HPCA conditions. Reaction

$$C_2H_5 \xrightarrow[*]{CH_4} C_2H_4^+ + H \quad D = 3.9 \text{ eV} \qquad (5)$$

5 is the major dissociation pathway in the single-collision CID mass spectrum of 2-keV $C_2H_5^+$ (Table I).

Table I. CID Mass Spectra of 2-keV Ions from CH_4[a]

CH_5^+		$C_2H_5^+$	
fragment ion	rel abund	fragment ion	rel abund
CH_4^+	100	$C_2H_4^+$	100
CH_3^+	39	$C_2H_3^+$	26
CH_2^+	5	$C_2H_2^+$	5
CH^+	1	C_2H^+	1
C^+	1		

[a] Reference 17.

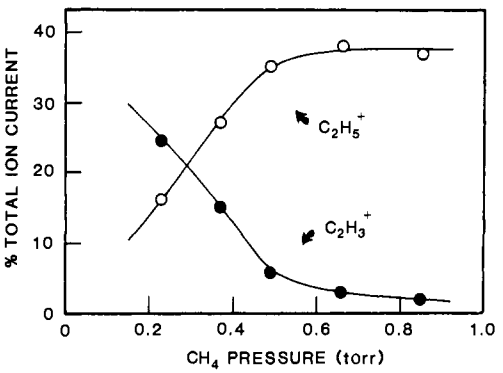

Figure 5. Relative abundances of $C_2H_5^+$ and $C_2H_3^+$ as a function of total pressure at a field strength in region 2 of 57 V/cm.

Under HPCA conditions, ions acquire internal energy gradually, in many collisions. If the unimolecular dissociation of the excited ions is sufficiently rapid and the energy differences between competing pathways are sufficiently large, ions will dissociate via the lower energy pathways before sufficient internal energy can be accumulated for the higher energy processes to occur. No $C_2H_4^+$, above the initial abundance, is observed in these experiments because the $C_2H_5^+$ dissociates via reaction 2 before it can be sufficiently activated to dissociate by reaction 5. Similarly, no $C_2H_6^+$ is produced in these experiments by the competing reaction, eq 6. The excited $C_2H_7^+$ dissociates by reaction 1b before enough additional energy is acquired for reaction 6 to occur.

$$C_2H_7^+ \xrightarrow[*]{CH_4} C_2H_6^+ + H \quad D = 3.8 \text{ eV} \qquad (6)$$

Reactions producing $C_2H_2^+$ and C_2H^+ directly from $C_2H_5^+$ are more endothermic and mechanistically difficult than reaction 5, which does not occur. Consequently, we feel that $C_2H_5^+$ does not dissociate directly to either $C_2H_2^+$ or C_2H^+ under HPCA conditions. By similar arguments, $C_2H_7^+$ does not dissociate directly to $C_2H_3^+$, $C_2H_2^+$, or C_2H^+ under HPCA conditions.

The effect of pressure of the reagent/collision gas on the dissociation of $C_2H_5^+$, reaction 4, is illustrated in Figure 5. The extent of dissociation decreases with increasing CH_4 pressure at a constant field strength in region 2. Similarly, the critical field strength for a given decomposition increases with increasing pressure.

Figure 6 shows the distributions of one-carbon ions in the HPCA mass spectrum of CH_4. The breakdown curves were

(12) Munson, M. S. B.; Field, F. H. *J. Am. Chem. Soc.* **1965**, *87*, 3294–3299.
(13) Burinsky, D. J.; Cooks, R. G.; Chess, E. K.; Gross, M. L. *Anal. Chem.* **1982**, *54*, 295–299.
(14) Douglas, D. J. *J. Phys. Chem.* **1982**, *86*, 185–191.
(15) Speranza, M.; Sefcik, M. D.; Henis, J. M. S.; Gaspar, P. P. *J. Am. Chem. Soc.* **1977**, *99*, 5583–5589.
(16) Leung, H.; Ichikawa, H.; Li, Y.; Harrison, A. G. *J. Am. Chem. Soc.* **1978**, *100*, 2479–2484.
(17) Field, F. H.; Franklin, J. L.; Munson, M. S. B. *J. Am. Chem. Soc.* **1963**, *85*, 3575–3583.

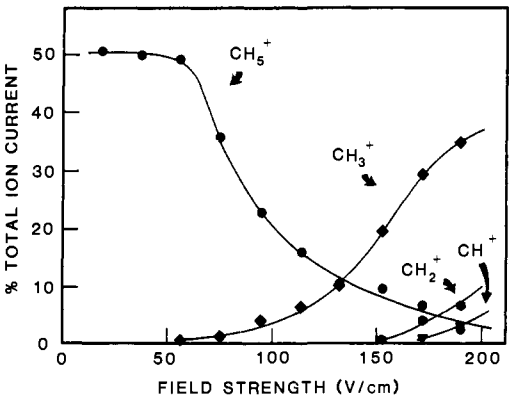

Figure 6. Relative abundances of one-carbon ions from CH_4 at a pressure of 0.50 torr as a function of field strength in region 2 of the two-region source.

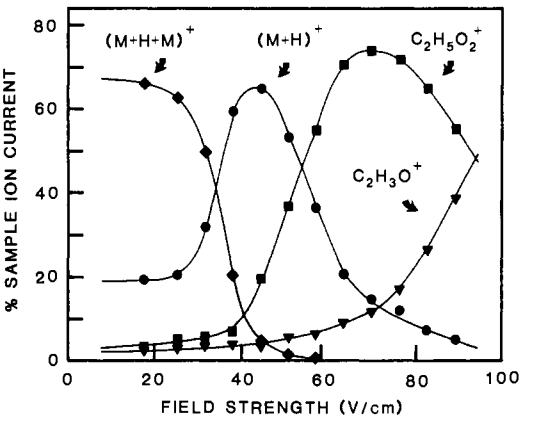

Figure 7. Relative abundances of sample ions from ethyl acetate in CH_4 at a total pressure of 0.40 torr as a function of field strength in region 2 of the two-region source.

acquired by varying the field strength in region 2 of the two-region source, as before. The ions, CH_5^+ and $C_2H_5^+$, comprise about 90% of the parent ion distribution for CH_4. Since CH_3^+, CH_2^+, and CH^+ are not significant products from the dissociation of $C_2H_5^+$ from CH_4/C_2H_6 mixtures, these ions must result primarily from the dissociation of CH_5^+. The dissociation sequence is shown in eq 7–9. The higher energy parallel dissociation pathway for

$$CH_5^+ \xrightarrow[*]{CH_4} CH_3^+ + H_2 \qquad D = 1.7 \text{ eV} \qquad (7)$$

$$CH_3^+ \xrightarrow[*]{CH_4} CH_2^+ + H \qquad D = 5.4 \text{ eV} \qquad (8)$$

$$CH_2^+ \xrightarrow[*]{CH_4} CH^+ + H \qquad D = 4.6 \text{ eV} \qquad (9)$$

CH_5^+ (eq 10) is not observed. There is, of course, the complication

$$CH_5^+ \xrightarrow[*]{CH_4} CH_4^+ + H \qquad D = 4.5 \text{ eV} \qquad (10)$$

that any CH_4^+ and CH_3^+ produced under HPCA conditions will react with CH_4 in subsequent collisions. In Figure 6, the initial increase in the relative abundance of CH_3^+ is smaller than the initial decrease in the relative abundance of CH_5^+, indicating that the CH_3^+ is reacting. The rate constants for the reactions of CH_4^+ and CH_3^+ with CH_4 are about the same; consequently, the ratio of ionic abundances, I_{16}/I_{15}, will be approximately proportional to the ratio of CH_4^+ and CH_3^+ produced by HPCA dissociation processes. This ratio is never greater than 0.03 in these experiments. This observation, as before, suggests that CH_5^+ dissociates via reaction 7 before sufficient energy can be accumulated for reaction 10 to occur. Reaction 10 is the dominant process for the single-collision decomposition of 2-keV CH_5^+ ions (Table I).

The internal energies of the ions increase with increasing field strength, but the relationship is not a simple one. At the critical field strength for the formation of an ion, the decomposing ions have acquired internal energies at least equal to the overall dissociation energy for the process (e.g., $C_2H_7^+ \rightarrow C_2H_5^+ \rightarrow C_2H_3^+$, D = 2.4 eV). In preliminary studies, log–log plots of overall dissociation energy vs. critical field strength gave the approximate relationship $D \propto E_c^{1.6}$. This result, however, depends on the length of region 2, the nature of the parent ion and the collision gas, and the pressure. Under well-defined drift conditions the drift velocities of ions are proportional to the field strength divided by pressure, E/P. The internal energies of the ions are not uniquely determined by the value of E/P under our experimental conditions. HPCA spectra at different pressures and the same E/P have different extents of dissociation. More complete studies of these relationships will be reported later.

The HPCA mass spectra for $C_2H_5^+$ and CH_5^+ differ sharply from the single-collision CID spectra given in Table I. The CH_4 HPCA mass spectra of esters, on the other hand, are similar to MIKES spectra of the protonated esters. Figure 7 shows the breakdown curves for the ions in the CH_4 HPCA mass spectrum of ethyl acetate. The first dissociation step is the desolvation of the abundant protonated dimer (eq 11). The large abundance

$$(M + H + M)^+ \xrightarrow[*]{CH_4} (M + H)^+ + M \qquad (11)$$

of the dimer at low-field strengths in region 2 results from the very long reaction time in region 1 and a relatively large concentration of ethyl acetate. Similar desolvation reactions have been observed under analogous conditions previously.[7] The consecutive dissociation reactions are

$$(C_2H_5O_2CCH_3 + H)^+ \xrightarrow[*]{CH_4} CH_3CO_2H_2^+ \qquad D = 1.1 \text{ eV} \qquad (12)$$

$$CH_3CO_2H_2^+ \xrightarrow[*]{CH_4} CH_3CO^+ + H_2O \qquad D = 2.0 \text{ eV} \qquad (13)$$

These dissociation products are the same as are observed in the 8-keV MIKES spectrum of protonated ethyl acetate given in Table II. Since dissociation product distributions are sensitive to experimental conditions under both single-collision and high-pressure CA conditions, meaningful quantitative comparisons of the spectra cannot be made.

Table II. MIKES Spectrum of 8-keV Protonated Ethyl Acetate[a]

fragment ion	m/z	rel abund[b]
$C_2H_3O^+$	43	2
$C_2H_5O_2^+$	61	100

[a] Reference 4. [b] Fragment ions less than 2% relative abundance not shown.

The low-pressure FT MS–CID spectrum of protonated 3-heptanone[18] and the CH_4 HPCA spectrum of 3-heptanone (field strength = 75 V/cm, CH_4 pressure = 0.4 torr) are compared in Figure 8. The FT MS–CID spectrum, Figure 8a, contains abundant fragment ions at m/z 97, 85, 84, 72, 69, 59, and 55, all of which result from direct dissociation of the protonated parent ion. Of these ions, only m/z 59 and 55 are observed as major products in the CH_4 HPCA spectrum, Figure 8b. These two ions, then, must be produced by the lowest energy dissociation pathways of protonated 3-heptanone. The ions resulting from higher energy processes are not observed as important products. The additional lower mass ions in the HPCA spectrum, m/z 45, 43, 39, 31, and 29, result from stepwise dissociation processes.

No broadening of parent or fragment ion peaks is noted at high-field strengths under HPCA conditions. Both parent and fragment ions can be characterized by high-resolution mass spectrometry and precise mass determinations. The signal at m/z 43 in the HPCA spectrum of 3-heptanone was resolved into two components, $C_2H_3O^+$ and $C_3H_7^+$, in roughly equal abundances. The peak at m/z 57 was also resolved into two components, with the major component being $C_3H_5O^+$ and the minor component

(18) White, R. L.; Wilkins, C. L. *Anal. Chem.* **1982**, *54*, 2211–2215.

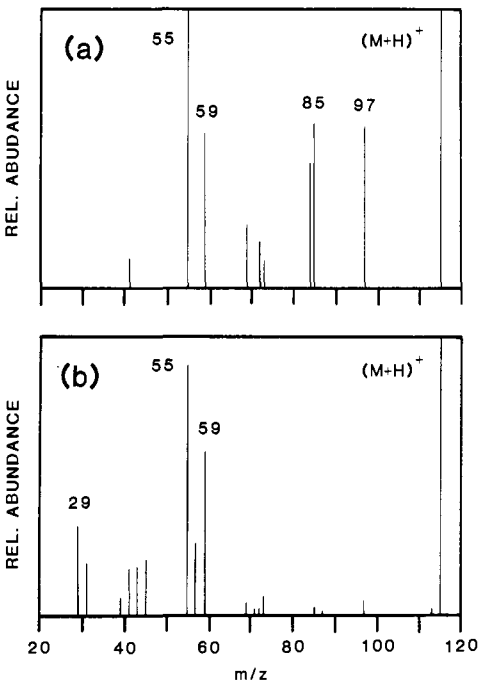

Figure 8. (a) FT MS–CID mass spectrum of protonated 3-heptanones;[18] (b) CH_4 HPCA mass spectrum of 3-heptanone at a total pressure of 0.40 torr and a field strength of 75 V/cm in region 2 of the two-region source.

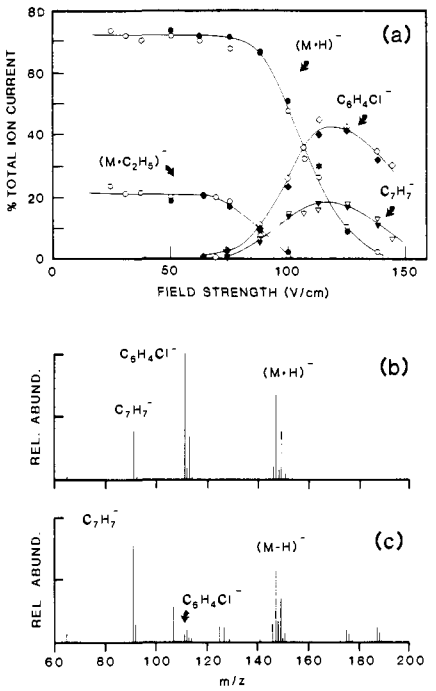

Figure 9. (a) Relative abundances of the major sample ions from dichlorobenzenes in CH_4 at a total pressure of 0.4 torr as a function of field strength in region 2 of the two-region source: open symbols, *o*-dichlorobenzene; solid symbols, *m*-dichlorobenzene. (b) CH_4 HPCA mass spectrum of *m*-dichlorobenzene with two-region source. (c) CH_4 HPCA mass spectrum of *m*-dichlorobenzene with three-region source.

$C_4H_9^+$. Precise mass measurements verified that m/z 59 was $C_3H_7O^+$ and m/z 55 was $C_4H_7^+$.

Figure 9a shows the breakdown curves for *o*- and *m*-dichlorobenzene under CH_4 HPCA conditions. The ionic distributions of the major dissociation ions are essentially the same for the two isomers. The major dissociation pathway is clearly the loss of HCl from the protonated species (eq 14). The decomposition of the adduct ion, $(M + C_2H_5)^+$, occurs at very slightly lower critical field strength than decomposition of the protonated ion. However, there is no obvious simultaneous increase in the protonated ion to establish the occurrence of the reaction

$$(C_6H_4Cl_2 + H)^+ \xrightarrow[*]{CH_4} C_6H_4Cl^+ + HCl \qquad (14)$$

$$(C_6H_4Cl_2 + C_2H_5)^+ \xrightarrow[*]{CH_4} (C_6H_4Cl_2 + H)^+ + C_2H_4$$

and the dissociation may proceed directly to $C_6H_4Cl^+$:

$$(C_6H_4Cl_2 + C_2H_5)^+ \xrightarrow[*]{CH_4} C_6H_4Cl^+ + C_2H_5Cl \qquad (15)$$

The ion at m/z 91, $C_7H_7^+$, appears at the same critical field strength as $C_6H_4Cl^+$, and the ratio of ionic abundances, $I_{C_7H_7^+}/I_{C_6H_4Cl^+}$, remains essentially constant (0.47 ± 0.09) at all field strengths. This ion is probably formed by subsequent reaction of $C_6H_4Cl^+$ with CH_4 (eq 16). This reaction is analogous to known reactions of $C_6H_5^+$ with CH_4 to give $C_7H_7^+$.[15,16]

$$C_6H_4Cl^+ + CH_4 \rightarrow C_7H_7^+ HCl \qquad (16)$$

The extent of reaction 16 can be increased by reconfiguring the ion source to the three-region mode shown in Figure 1b. In the three-region source, fragment ions produced in region 2 are allowed to react with the reagent/collision gas in a region of low-field strength, region 3, before leaving the source. The reaction sequence 14 followed by reaction 16 is established by comparison of the HPCA spectra in the two-region source, Figure 9b, and three-region source, Figure 9c. In the three-region source $C_6H_4Cl^+$ has essentially disappeared and $C_7H_7^+$ has increased significantly in relative abundance. In addition to $C_7H_7^+$, several new ions are also observed. The proposed sequence of reactions occurring in region 3 is shown in Scheme I. The distribution of product ions from reactions in region 3 is sensitive to the field strength in region

Scheme I

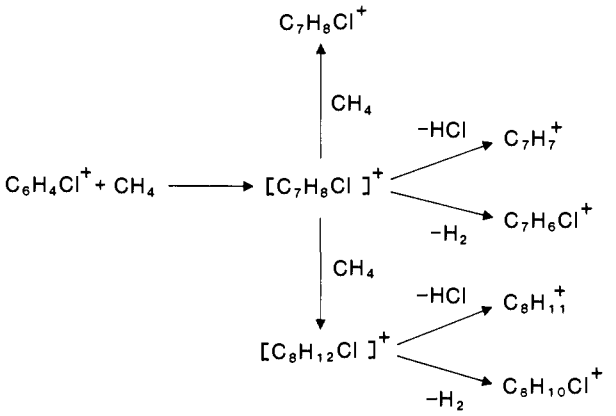

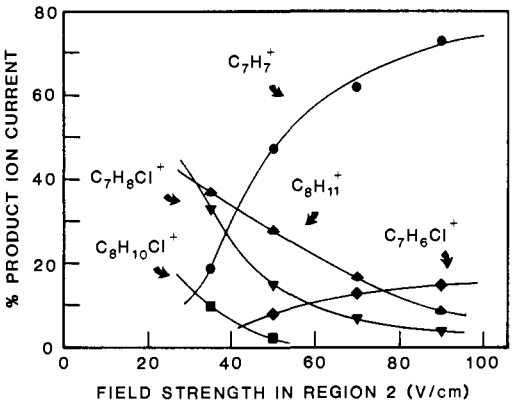

Figure 10. Relative abundances of products from subsequent reactions of $C_6H_4Cl^+$ with CH_4 in region 3 as a function of field strength in region 2 of the three-region source.

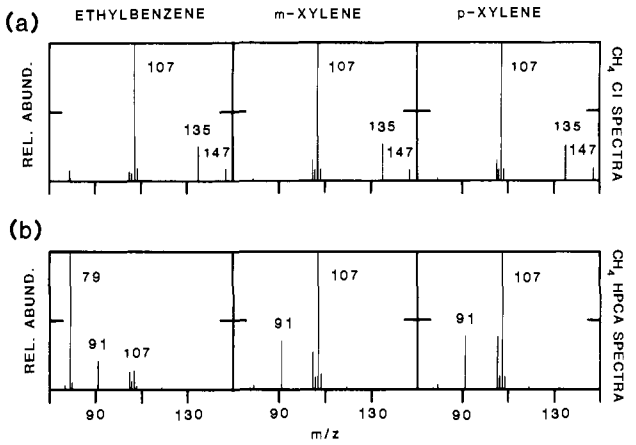

Figure 11. (a) CH_4 CI masss spectra of ethylbenzene, *m*-xylene, and *p*-xylene. (b) CH_4 HPCA mass spectra of ethylbenzene, *m*-xylene, and *p*-xylene under identical conditions.

2. Figure 10 shows the relative distributions of subsequent reaction product ions as a function of field strength in region 2. The ions, $C_7H_7^+$ and $C_7H_6Cl^+$, that result from decomposition of the first excited intermediate, $[C_7H_8Cl^+]^*$, increase in relative abundance with increasing field strength in region 2. The ratio of elimination products, $I_{C_7H_6Cl^+}/I_{C_7H_7^+}$, is approximately constant (0.19 ± 0.02). Those products requiring third-body stabilization or reaction with a second CH_4 ($C_7H_8Cl^+$, $C_8H_{11}^+$, and $C_8H_{10}Cl^+$) decrease in relative abundance with increasing field strength in region 2. These results clearly indicate a decrease in the lifetime of the first excited intermediate, $[C_7H_8Cl^+]^*$, with increasing field strength in region 2 and suggest that $C_6H_4Cl^+$ leaves region 2 with more excess energy, both kinetic and internal, at higher field strengths.

The CH_4 CI and two-region HPCA spectra of ethylbenzene and *p*- and *m*-xylene under identical conditions are given in Figure 11. The CH_4 CI spectra are very similar for all three compounds: predominantly protonated sample with lesser amounts of $(M + C_2H_5)^+$ and $(M + C_3H_5)^+$. The CI spectra of ethylbenzene and the xylenes are perhaps differentiable by the larger abundance of m/z 79 in the ethylbenzene spectrum and m/z 105 in the spectra of the xylenes. The differences are not large, however. The ethylbenzene and xylene HPCA spectra are clearly differentiable and can be interpreted in terms of structural differences of the protonated ions.

The major dissociation pathway for protonated ethylbenzene is clearly

$$(C_6H_5C_2H_5 + H)^+ \xrightarrow[*]{CH_4} C_6H_7^+ + C_2H_4 \qquad D = 1.5 \text{ eV} \tag{17}$$

The major dissociation pathway for the protonated xylenes is

$$(C_6H_4(CH_3)_2 + H)^+ \xrightarrow[*]{CH_4} C_7H_7^+ + CH_4 \qquad D = 1.3 \text{ eV} \tag{18}$$

The $(M + H)^+$ ions for alkyl aromatic hydrocarbons are ring-protonated species. The elimination of CH_4 from protonated xylene via reaction 18 can involve a hydrogen from either the ring or the second methyl group. The $C_7H_7^+$ produced in the HPCA of xylene does not react with CH_4 in the three region source. This nonreactivity indicates that $C_7H_7^+$ is a benzyl or tropylium ion rather than a methylphenyl ion, and hydrogen extraction occurs from the methyl group or there is a rapid rearrangement of the fragment ion. The extents of dissociation of the protonated xylenes are significantly less than for ethylbenzene even though their calculated dissociation energies (assuming $C_7H_7^+$ is the benzyl ion) are slightly lower than that for ethylbenzene. This observation suggests that a large activation energy is involved in the elimination of CH_4 from the protonated xylenes.

The CH_4 HPCA spectra for the isomeric xylenes are very similar, as they were for the isomeric dichlorobenzenes. Differentiating positional isomers by HPCA may not be possible.

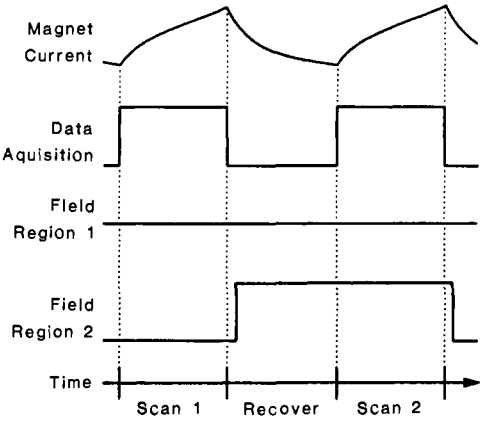

Figure 12. Timing sequence for simultaneous CI/CA mass spectrometry.

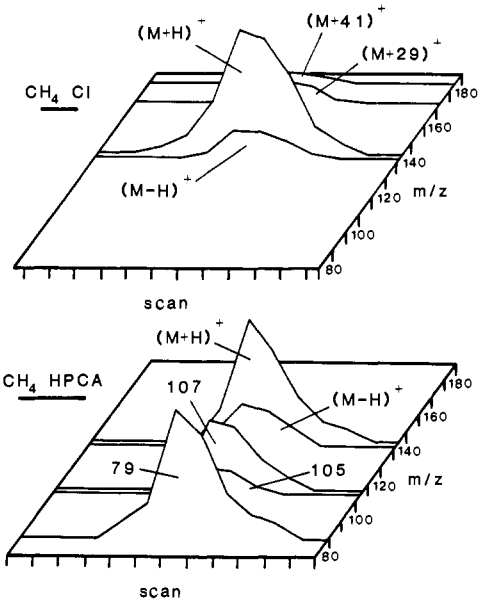

Figure 13. Reconstructed CH_4 CI and CH_4 HPCA ion chromatograms for diethylbenzene obtained "simultaneously" across the same GC peak.

Simultaneous CI/CA Mass Spectrometry

The field strength in region 2 of the two-region source can be changed rapidly, making it possible to acquire spectra with widely differing extents of dissociation on consecutive scans of the mass spectrometer. We have developed a simple system that automatically switches the field strength in region 2 between two preset values on alternate scans of the mass spectrometer. This system has been used to obtain alternate CI spectra with very little dissociation and HPCA spectra with very large extents of dissociation. The experiment is shown schematically in Figure 12. The mass spectra are obtained with a minicomputer on the upscan of the mass spectrometer magnet. A constant low-field strength, 5–10 V/cm, is maintained in region 1 throughout the experiment. During scan 1 the field strength in region 2 is low and a CI mass spectrum is acquired. Immediately after the scan is completed the field strength in region 2 is automatically "stepped up", and the source has several seconds to stabilize while the magnet recovers. During scan 2 an HPCA mass spectrum is acquired. After the scan is completed the field strength is automatically "stepped down", the source recovers, and the cycle repeats. No studies have been done yet to determine how quickly the source can recover between scans, but recovery times of less than 1 s may be possible.

This technique is most useful when used with GC sample introduction where it can provide molecular weight information from the CI spectra and structural information from the HPCA spectra across a single GC peak. Figure 13 shows reconstructed CH_4 CI and HPCA ion chromatograms that were obtained "simultaneously" across the same GC peak for diethylbenzene.

The CI ion chromatogram contains the ususal CH_4 CI ions: predominantly protonated diethylbenzene and smaller amounts of $(M - H)^+$, $(M + C_2H_5)^+$, and $(M + C_3H_5)^+$. The HPCA spectra contain several fragment ions diagnostic of the structure of the sample with the major dissociation pathways being

$$(C_6H_4(C_2H_5)_2 + H)^+ \xrightarrow[*]{CH_4} (C_6H_5(C_2H_5) + H)^+ + C_2H_4 \quad (19)$$

and

$$(C_6H_5(C_2H_5) + H)^+ \xrightarrow[*]{CH_4} C_6H_7^+ + C_2H_4 \quad (20)$$

HPCA mass spectra acquired at a fixed extent of dissociation cannot provide the detailed structural information obtained from a breakdown curve. However, when combined with the CI mass spectra and GC retention times, the HPCA data provide a potentially powerful additional dimension in sample characterization.

Acknowledgment is made to the donors of the Petroleum Research Fund, administered by the American Chemical Society, for support of this research.

Registry No. CH_4, 74-82-8; C_2H_6, 74-84-0; ethyl acetate, 141-78-6; 3-heptanone, 106-35-4; *o*-dichlorobenzene, 95-50-1; *m*-dichlorobenzene, 541-73-1; ethylbenzene, 100-41-4; *m*-xylene, 108-38-3; *p*-xylene, 106-42-3.

EPR Evidence on Molecular and Electronic Structure of Nitrogen Trifluoride Radical Cation

Alvin M. Maurice,[†] R. Linn Belford,*[†] Ira B. Goldberg,*[‡] and Karl O. Christe[§]

Contribution from the School of Chemical Sciences, University of Illinois, Urbana, Illinois 61801, Rockwell International Science Center, Thousand Oaks, California 91360, and Rocketdyne Division, Rockwell International, Canoga Park, California 91304. *Received April 26, 1982*

Abstract: Computer simulations of the EPR spectra of rigid $^{14}NF_3^+\cdot$ and $^{15}NF_3^+\cdot$ trapped in powdered NF_4AsF_6 at 25 K show characteristics of a trigonal pyramid with the following *principal* values for the coupling matrices: $|g(\parallel,\perp)| = 2.003$; $|A_{^{14}N}(\parallel,\perp)| = 324, 187$ MHz; $A_{^{15}N}(\parallel,\perp)| = 451, 260$ MHz; $A_{^{19}F}(z,x,y) = 880, 340, 360$ MHz; α, the angle between parallel axes for A_F and $A_{N'} = 15°$. The nitrogen p:s spin-density ratio (computed from the nitrogen hyperfine splittings) is consistent with $sp^{2.5}$ nitrogen hybrids in the NF bonds and with a pyramid angle of about 105°. Although the same pyramid angle appears to agree with the orientation of the principal axis of the fluorine hyperfine coupling matrix ($|\alpha| = 15°$, pyramid angle = 90° + $|\alpha|$), electronic structure computations imply that α is negative and that the agreement is fortuitous. Some comparisons are made with isoelectronic radicals BF_3^- and CF_3—the latter being essentially tetrahedral with sp^3 hybridization.

Goldberg, Crowe, and Christe have presented high- and low-temperature EPR spectra of the radical cations $^{14}NF_3^+\cdot$ and $^{15}NF_3^+\cdot$ produced by γ-irradiation of NF_4AsF_6.[1] Their analyses properly accounted for the high-temperature (~240 K) spectra, but computational limitations prevented a complete analysis of the low-temperature (~25 K) EPR spectra, which are drastically different. At the high temperature, the molecule is axially symmetric, apparently spinning freely, probably both about its threefold axis and about an axis nearer to the F_3 plane. In contrast, at the low temperature, each molecule appears to be locked into a fixed orientation and the EPR spectra are, as expected, much more complex. Now, with an appropriately modified computer simulation program, we are able to interpret these low-temperature spectra.

Several studies providing information on hyperfine coupling, spin density, and geometry of the isoelectronic species $BF_3^-\cdot$[2] and $CF_3\cdot$ have been published.[3-7] The opportunity to compare those bonding features that can be deduced from hyperfine matrices of the isoelectronic series provides one of the motivations for the study of NF_3^+. Here we describe our interpretation of the low-temperature EPR spectra and draw conclusions regarding geometry and bonding in the nitrogen trifluoride radical cation.

Experiments and Computation

Low-temperature EPR spectra of $^{14}NF_3^+$ and $^{15}NF_3^+$ have been described[1] as have the synthesis, experimental conditions, and the spectrometer used in this work. The spectra chosen for the current analysis are reproduced in the figures.

Simulated EPR spectra are generated by means of the program "POWD" running on the VAX 11/780 computer connected to a Houston Instruments HIPLOT digital plotter. Program POWD has its origins in an EPR powder simulation program, kindly provided by Dr. J. R. Pilbrow of Monash University, which employs second-order perturbation theory for the first nucleus and first-order approximations for superhyperfine terms. It was revised by White and Belford[8,9] and Chasteen et al.[10] into EPRPOW. Nilges and Belford[11,12] rewrote this program as POW to employ more efficient angular sampling (to minimize the unevenness of point density on the sphere) and integration technique four-point Gauss quadrature).[13] The version of POWD that we have created for the current work is a substantially modified POW that uses a perturbation method accurate to second order in all hyperfine terms (including internuclear cross-terms)[14] to calculate a powder spectrum for a spin $S = {}^1/_2$ system with up to four hyperfine nuclei. Program POWD permits principal axes of all four hyperfine nuclei interaction matrices as well as those of the

[†] University of Illinois.
[‡] Rockwell International Science Center.
[§] Rocketdyne Division.

(1) I. B. Goldberg, H. R. Crowe, and K. O. Christe, *Inorg. Chem.*, **17**, 3189 (1978).
(2) R. L. Hudson and F. Williams, *J. Chem. Phys.*, **65**, 3381 (1976).
(3) R. W. Fessenden, *J. Magn. Reson.*, **1**, 277 (1969).
(4) R. W. Fessenden and R. H. Schuler, *J. Chem. Phys.*, **43**, 2704 (1965).
(5) M. T. Rogers and L. D. Kispert, *J. Chem. Phys.*, **46**, 3193 (1967).
(6) J. Maruani, J. A. R. Coope, and C. A. McDowell, *Mol. Phys.*, **18**, 165 (1970).
(7) J. Maruani, C. A. McDowell, H. Nakajima, and P. Raghunathan, *Mol. Phys.*, **14**, 349 (1968).
(8) L. K. White and R. L. Belford, *J. Am. Chem. Soc.*, **98**, 4428 (1976).
(9) L. K. White, Ph.D. Thesis, University of Illinois, Urbana, 1975.
(10) N. F. Albanese and N. D. Chasteen, *J. Phys. Chem.*, **82**, 910 (1978).
(11) M. J. Nilges and R. L. Belford, *J. Magn. Reson.*, **35**, 259 (1975).
(12) M. J. Nilges, Ph.D. Thesis, University of Illinois, Urbana, 1979.
(13) R. L. Belford and M. J. Nilges, "Computer Simulation of EPR PowderSpectra", Symposium on Electron Paramagnetic Resonance Spectroscopy, Rocky Mountain Conference on Analytical Chemistry, Denver, August 1979.
(14) J. A. Weil, *J. Magn. Reson.*, **18**, 113 (1975).

0002-7863/83/1505-3799$01.50/0